Path Planning for UAV Target Tracking with Non-Gaussian Noise

Yuemei Qin, Yuanyuan Xu, Yang Liu

Abstract—**Target tracking of UAV typically assumes that the system model is linear and disturbed by Gaussian noise. However, in practical applications, the tracking performance significantly deteriorates when encountering non-Gaussian noise, particularly when system measurements rely on nonlinear parameters (such as range and bearing). To address this problem, this paper proposes an extended target tracking method incorporating path planning, which utilizes mobile UAV equipped with angle-of-arrival (AOA) sensors to achieve GPS-denied maneuvering target tracking. Firstly, the maximum correntropy criterion extended Kalman filter (MCCEKF) is utilized to improve the accuracy of state estimation by maximizing the correlated entropy between the state estimate and the observed data. Secondly, particle swarm optimization (PSO) is utilized to optimize the UAV's path synchronously based on state estimate to obtain more effective measurements. Finally, the maximum correntropy criterion extended Kalman filter-particle swarm optimization (MCEP) is designed to estimate the system state accurately. Simulation experiments are presented to demonstrate the accuracy and robustness of the proposed method for UAV target tracking with non-Gaussian noise.**

Index Terms—**Target tracking, Path planning, Maximum Correntropy Criterion, Non-Gaussian noise**

I. Introduction

In recent years, target tracking of unmanned aerial vehicles (UAV) has a wide range of applications in fields such as aviation, military, and security with the rapid advancement of UAV technology [1]. However, UAV tracking systems in complex operational environments typically encounter GPS-denied (no global positioning system) scenarios, which cause the system measurement model to be nonlinear, angle-of-arrival (AOA) measurements from radiation sources have emerged as a crucial parameter for localization and tracking under such circumstances [2]. Consequently, UAVs are typically equipped with AOA sensors for target tracking to address these challenges. Additionally, the system noise exhibits a non-Gaussian distribution due to interference from radar systems and radio frequency transmissions. Thus, the system is generally nonlinear and disturbed by non-Gaussian noise under practical working conditions [3].

To address nonlinear system filtering challenges, maximum likelihood estimation (MLE) [4] and the pseudo-linear estimator (PLE) [5] can be utilized to approximate the linearization of the system and apply standard linear filtering algorithms to solve nonlinear filtering. MLE linearizes the model around the optimal parameters obtained by optimizing the likelihood function, whereas PLE linearizes the system locally through optimization of iterative updates. Additionally, algorithms based on Kalman filter (KF) are widely applied including extended Kalman filter (EKF) [6], unscented Kalman filter (UKF) [7], and pseudo-linear Kalman filter (PLKF) [8]. EKF employs Taylor series expansion for local linearization of nonlinear systems, whereas UKF propagates nonlinearity of the system through selecting a set of "sigma points". PLKF focuses on linearizing the nonlinear state or measurement equations directly. The methods mentioned can effectively address nonlinear system filtering problems with Gaussian noise. However, when the system is nonlinear and disturbed by non-Gaussian noise, the accuracy of UAV target tracking degrades significantly.

To address the target tracking challenges under non-Gaussian noise conditions, various algorithms have been proposed including the particle filter (PF) [9] and the H-infinity (H∞) filter [10]. The PF utilizes a set of random particles to approximate the posterior probability distribution of system state variables, which allows it to effectively handle the complexity of non-Gaussian noise. The H∞ filter exhibits remarkable adaptability to diverse noise types due to its independence from statistical characteristics such as mean and covariance. Additionally, optimization criteria derived from information theoretic learning (ITL) [11] have emerged as promising approaches in recent years, such as maximum correntropy criterion (MCC) [12] and minimum error entropy criterion (MEE) [13]. MCC leverages kernel functions to quantify the similarity between estimation errors and true values to suppress outliers in non-Gaussian noise scenarios. MEE minimizes error entropy to implement robust processing of non-Gaussian noise, which enables it not to make specific assumptions about noise distribution.

In order to enhance the accuracy of UAV maneuvering target tracking, the target tracking performance can be significantly improved by optimizing the UAV flying path to make information gathered from measurements more effective. Accordingly, a cost function has been designed for UAV path planning, including the estimation covariance matrix [14] and the Fisher information matrix (FIM) [15] typically. The estimation covariance matrix describes the uncertainty of state estimates, whereas FIM quantifies the

Manuscript received December 3, 2024; revised August 3, 2025.

This work was supported in part by Natural Science Foundation of Shaanxi Province, 2021JQ-702.

Yuemei Qin is lecturer of School of Automation, Xi'an University of Posts & Telecommunications, Xi'an 710121, China. (e-mail: qinyuemei@xupt.edu.cn).

Yuanyuan Xu is a graduate student of School of Automation, Xi'an University of Posts & Telecommunications, Xi'an 710121, China. (e-mail: forever187411@gmail.com).

Yang Liu is lecturer of School of Automation, Xi'an University of Posts & Telecommunications, Xi'an 710121, China. (e-mail: yyangbrand@163.com).

"information content" of the measurement information with respect to parameter estimation [16]. Various algorithms have been investigated for UAV path planning including Dijkstra [17], A* [18], and particle swarm optimization (PSO) [19]-[20]. Dijkstra employs an incremental approach to update the shortest paths by leveraging previously identified optimal routes. A* incorporates a heuristic function that provides additional search guidance, enabling more efficient identification of shortest paths by prioritizing promising trajectories toward the target node on the foundation of Dijkstra. PSO explores the solution space through the collective movement of particle populations to discover optimal path solutions.

To solve the problem of UAV maneuvering target tracking in the nonlinear systems with non-Gaussian noise, the maximum correntropy criterion extended Kalman filter-particle swarm optimization (MCEP) is proposed based on the above discussion. The proposed method integrates two key components: (1) maximum correntropy criterion extended Kalman filter (MCCEKF) is utilized to obtain the current state estimation under the nonlinear system with non-Gaussian noise. (2) particle swarm optimization (PSO) is utilized to plan the optimal path of the system based on the filtering estimation results. Finally, the new measurement information is obtained to enhance the stability and accuracy of UAV target state estimation based on the optimal path for the next state estimation. The simulation results demonstrate that the system state estimation can be performed quickly and accurately with the assistance of PSO, which improves estimation accuracy and provides new directions for future research.

The rest of this paper is organized as follows: Section II formulates the target tracking problem under non-Gaussian conditions. Section III details the MCCEKF derivation and PSO implementation for trajectory planning. Section IV presents the simulation experiments and analysis. Section V concludes with research contributions and future directions.

In this paper, the symbol '$=:$' denotes definition, 'I' and 'O' are the identity matrix and zero matrices with appropriate dimensions respectively, '$[\bullet]^T$' and '$[\bullet]^{-1}$' represents matrix transpose and inverse respectively, 'k' represents the measurement time index, '$\mathbb{R}$' is the space formed by real-valued vectors, '$diag(\bullet)$' represents a diagonal matrix, '$\|\bullet\|_2$' represents the L2 norm, '$\exp(\bullet)$' denotes the natural exponential function, and '$tr(\bullet)$' indicates the trace of a matrix.

II. Problem Formulation

This paper considers a 2D target tracking problem utilizing a mobile UAV equipped with AOA sensors in a GPS-denied environment. As shown in Figure 1, the positions and velocities of the UAV and target are unknown in $O-\xi\eta$.

To achieve state estimation under GPS-denied environments, we select two static anchors (such as buildings or trees) at $b_1 =: [\xi_{b1}, \eta_{b1}]^T$, $b_2 =: [\xi_{b2}, \eta_{b2}]^T$, the position of UAV at time k is $u(k) =: [\xi_u(k), \eta_u(k)]^T$, target location is $t(k) =: [\xi_t(k), \eta_t(k)]^T$, and target velocity is $t_v(k) =: [\dot{\xi}_t(k), \dot{\eta}_t(k)]^T$. For ease of understanding, Figure 1 illustrates the self-positioning and target tracking of UAV during path planning.

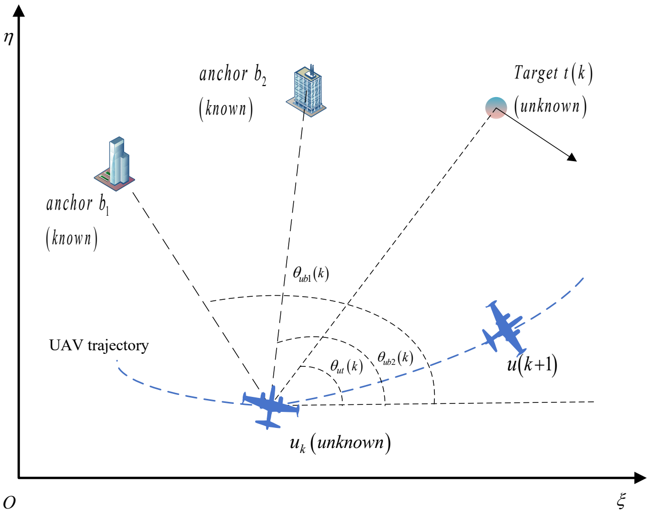

Fig. 1. Self-positioning and target tracking of UAV with path planning.

In Figure 1, the UAV measures three angles at kth including two relative to static anchors $\theta_{ub1}(k)$, $\theta_{ub2}(k)$ and one relative to the target $\theta_{ut}(k)$.The measurement vector $Z(k) =: [\tilde{\theta}_{ub1}(k), \tilde{\theta}_{ub2}(k), \tilde{\theta}_{ut}(k)]^T$ is represented as:

$$\tilde{\theta}_{ub1}(k) = \tan^{-1}\left(\frac{\eta_{b1} - \eta_u(k)}{\xi_{b1} - \xi_u(k)}\right) + v(k) \tag{1}$$

$$\tilde{\theta}_{ub2}(k) = \tan^{-1}\left(\frac{\eta_{b2} - \eta_u(k)}{\xi_{b2} - \xi_u(k)}\right) + v(k) \tag{2}$$

$$\tilde{\theta}_{ut}(k) = \tan^{-1}\left(\frac{\eta_t(k) - \eta_u(k)}{\xi_t(k) - \xi_u(k)}\right) + v(k) \tag{3}$$

where the $\tan^{-1}$ is a four-quadrant inverse tangent, and the $v(k)$ represents the non-Gaussian noise, which satisfies $N(0, R(k))$.

Note: Non-Gaussian noise is presented in radar measurements such as impulsive noise and α-stable noise, which exhibit heavy-tailed characteristics with longer tails and Gaussian-like central region. Such non-Gaussian noise can be decomposed into a weighted sum of Gaussian noise and noise with 'heavy-tailed' characteristics. In this paper, the Gaussian mixture noise model with distinct variances is utilized to represent the non-Gaussian noise:

$$v(k) \sim (1-\vartheta)N(u_1, \gamma_1) + \vartheta N(u_2, \gamma_2) \tag{4}$$

where $0 \le \vartheta < 1$ represents the intensity of the heavy-tail noise, $N(u_1, \gamma_1)$ denotes Gaussian noise with mean u_1 and variance γ_1, $N(u_2, \gamma_2)$ represents Gaussian noise with a large variance.

First, the state and measurement vectors of the system are formulated in the discrete time domain as follows:

$$X(k+1) = F(k)X(k) + \omega(k) \tag{5}$$

$$Z(k)=H(k)X(k+1)+v(k) \tag{6}$$

where $X(k)\in\mathbb{R}^n$ and $Z(k)\in\mathbb{R}^m$ represent the state vector and measurement vector of the system at kth respectively, $F(k)$ is the state transition matrix, and $H(k)$ is the measurement matrix. $\omega(k)\in\mathbb{R}^n$ denotes process noise, and $v(k)\in\mathbb{R}^m$ denotes measurement noise. $\omega(k)$ follows a normal distribution with zero mean and variance $Q(k)$, whereas $v(k)$ follows a Laplace distribution with zero mean and variance $R(k)$, the process noise and measurement noise are uncorrelated. The system state is defined as $X(k)=\left[\xi_u(k),\dot{\xi}_u(k),\eta_u(k),\dot{\eta}_u(k),\xi_t(k),\dot{\xi}_t(k),\eta_t(k),\dot{\eta}_t(k)\right]^T$ at discrete time k, and the UAV location and velocity are $\xi_u(k)$, $\eta_u(k)$, $\dot{\xi}_u(k)$, $\dot{\eta}_u(k)$ in the ξ and η directions, the target location and velocity is $\xi_t(k)$, $\eta_t(k)$, $\dot{\xi}_t(k)$, $\dot{\eta}_t(k)$ in the ξ and η directions. ψ represents the sampling period, and transition matrix $F(k)$ is defined as:

$$F(k)=\begin{bmatrix} F_i & O & O & O \\ O & F_i & O & O \\ O & O & F_i & O \\ O & O & O & F_i \end{bmatrix} \tag{7}$$

$$F_i=\begin{bmatrix} 1 & \psi \\ O & 1 \end{bmatrix} \tag{8}$$

For the aforementioned system model (5)-(7), a significant decline and instability in filtering performance of the existing EKF for tracking maneuvering targets emerge due to the neglect of non-Gaussian noise effects and the uncertainty of the system measurement state. To solve the problem of non-Gaussian noise and measurement state uncertainty in maneuvering target tracking under a GPS-denied environment, the MCEP is proposed to estimate the target state with the assistance of UAV path planning. Firstly, MCCEKF is employed to achieve high-precision filtering results under non-Gaussian noise. Secondly, PSO is utilized to correct the system states to reduce the impact on maneuvering target tracking. Therefore, the MCEP enables precise estimation of target states.

III. Path Planning Based on Particle Swarm Optimization under Maximum Correntropy Extended Kalman Filtering

In this section, MCCEKF is utilized to achieve state estimation of the nonlinear system under non-Gaussian noise conditions. PSO is utilized to obtain the optimal solution for single-step path planning by optimizing the cost function based on the aforementioned state estimation. In general, this method effectively improves the accuracy of system tracking and enhances its stability and practicality in non-Gaussian noise environments.

A. Extended Kalman Filter based on Maximum Correntropy Criterion

To solve the performance degradation in maneuvering target tracking under non-Gaussian noise, MCCEKF is designed from aspects such as state prediction, measurement equation formulation, and state updating, which adopts the robust MCC as the optimality criterion instead of employing the MMSE. The recursive process of the MCCEKF algorithm from time k to time $k+1$ is presented as follows.

Initially, the prior state and covariance estimates are obtained according to equations (9) and (10).

$$\hat{X}(k|k-1)=F(k-1)\hat{X}(k-1|k-1) \tag{9}$$

$$\begin{aligned}\hat{P}(k|k-1)=F(k-1)\hat{P}(k-1|k-1)\\ F^T(k-1)+Q(k-1)\end{aligned} \tag{10}$$

Calculate the Jacobian matrix $H(k)$ based on the current state and measurement.

$$H(k)=\begin{bmatrix} \frac{\eta_{b1}-\eta_u(k)}{d_{ub1}{}^2} & O & \frac{\xi_u(k)-\xi_{b1}}{d_{ub1}{}^2} & O & O & O & O & O \\ \frac{\eta_{b2}-\eta_u(k)}{d_{ub2}{}^2} & O & \frac{\xi_u(k)-\xi_{b2}}{d_{ub2}{}^2} & O & O & O & O & O \\ \frac{\eta_t(k)-\eta_u(k)}{d_{ut}{}^2} & O & \frac{\xi_u(k)-\xi_t(k)}{d_{ut}{}^2} & O & \frac{\eta_u(k)-\eta_t(k)}{d_{ut}{}^2} & O & \frac{\xi_t(k)-\xi_u(k)}{d_{ut}{}^2} & O \end{bmatrix} \tag{11}$$

where $d_{ub1}=\left\|u(k)-b_1\right\|_2$, $d_{ub2}=\left\|u(k)-b_2\right\|_2$, $d_{ut}=\left\|u(k)-t(k)\right\|_2$.

For the model described in the Section II, which yields a nonlinear regression model, we have:

$$\begin{bmatrix} \hat{X}(k|k-1) \\ Z(k) \end{bmatrix}=\begin{bmatrix} I \\ H(k) \end{bmatrix}X(k)+\alpha(k) \tag{12}$$

where $\alpha(k)$ is

$$\alpha(k)=\begin{bmatrix} -\left(X(k)-\hat{X}(k|k-1)\right) \\ v(k) \end{bmatrix} \tag{13}$$

with

$$\begin{aligned} E\left[\alpha(k)\alpha^T(k)\right]&=\begin{bmatrix} \hat{P}(k|k-1) & O \\ O & R(k) \end{bmatrix} \\ &=\begin{bmatrix} M_p(k|k-1)M_p{}^T(k|k-1) & O \\ O & M_r(k)M_r{}^T(k) \end{bmatrix} \\ &=M(k)M^T(k) \end{aligned} \tag{14}$$

where $M(k)$ is obtained by Cholesky decomposition of the covariance matrix $E\left[\alpha(k)\alpha(k)^T\right]$. Left-multiplying both sides of equation (12) by $M^{-1}(k)$, we obtain:

$$A(k)=W(k)X(k)+e(k) \tag{15}$$

where $A(k)=M^{-1}(k)\begin{bmatrix} \hat{X}(k|k-1) \\ Z(k) \end{bmatrix}$, $W(k)=M^{-1}(k)\begin{bmatrix} I \\ H(k) \end{bmatrix}$, $e(k)=M^{-1}(k)\alpha(k)$.

The MCCEKF optimizes covariance matrix through Cholesky decomposition, avoiding numerical instability and enhancing the filter's robustness against outliers.

For ease of understanding, Table I presents the implementation steps of MCCEKF including the filter initialization, prediction, iteration, and other processes. Where $a_i(k)$ denotes the ith row of $A(k)$, $w_i(k)$ denotes the ith row of $W(k)$, and $e_i(k)$ denotes the ith element of $e_i(k)$.

TABLE I
ALGORITHM PROCESS OF MCCEKF

```
Input: $\hat{X}(0|0)$, $\hat{P}(0|0)$
Output: $\hat{X}(k|k)$, $P(k|k)$
1: Initialization.
    $\hat{X}(k-1|k-1) \leftarrow \hat{X}(0|0)$                // Initial state estimate
    $\hat{P}(k-1|k-1) \leftarrow \hat{P}(0|0)$                // Initial covariance matrix
    $\sigma \leftarrow$ Kernel bandwidth
    $\varepsilon \leftarrow$ a small positive number
2: Prediction.
    $\hat{X}(k|k-1) \leftarrow F(k-1)\hat{X}(k-1|k-1)$            // Predicted state
    $\hat{P}(k|k-1) \leftarrow F(k-1)\hat{P}(k-1|k-1) F^T(k-1)+Q(k-1)$    // Predicted covariance
    $H(k) \leftarrow ComputeJacobian\left(\hat{X}(k|k-1)\right)$        // Jacobian matrix
3: Build regression model (Equation. 11).
    Perform Cholesky decomposition to obtain $M_p(k|k-1)$.
4: Fixed-Point Iteration.
    $t \leftarrow 1$
    $\hat{X}(k|k)_{t-1} \leftarrow \hat{X}(k|k-1)$          // Initialize fixed-point iteration
    $\hat{X}(k|k)_t \leftarrow$ state estimates in the fixed-point iteration t
5: The iteration process is performed to obtain $\hat{X}(k|k)_t$, $\hat{P}(k|k)_t$.
    $\hat{X}(k|k)_t = \hat{X}(k|k-1)+\tilde{K}(k)\left(Z(k)-H(k)\hat{X}(k|k-1)\right)$   (16)
    $\hat{P}(k|k)_t = \left(I-\tilde{K}(k)H(k)\right)\hat{P}(k|k-1) \left(I-\tilde{K}(k)H(k)\right)^T+\tilde{K}(k)R(k)\tilde{K}^T(k)$   (17)
    $\tilde{K}(k) = \tilde{P}(k|k-1)H^T(k) \left(H(k)\tilde{P}(k|k-1)H^T(k)+\tilde{R}(k)\right)^{-1}$   (18)
    $\tilde{P}(k|k-1) = M_p(k|k-1)\tilde{C}_x^{-1}(k)M_p^T(k|k-1)$   (19)
    $\tilde{R}(k) = M_r(k)\tilde{C}_y^{-1}(k)M_r^T(k)$   (20)
    $\tilde{C}_x(k) = diag\left(G_\sigma(\tilde{e}_1(k)),\cdots G_\sigma(\tilde{e}_n(k))\right)$   (21)
    $\tilde{C}_y(k) = diag\left(G_\sigma(\tilde{e}_{n+1}(k)),\cdots G_\sigma(\tilde{e}_{n+m}(k))\right)$   (22)
    $G_\sigma(e_i(k)) = \exp\left(-\frac{(e_i(k))^2}{2\sigma^2}\right)$   (23)
    $\tilde{e}_i(k) = a_i(k)-w_i(k)\hat{X}(k|k-1)_{t-1}$   (24)
6: Compare the state estimates at iteration step $t$ and step $t-1$.
    If $\frac{\left\|\hat{X}(k|k)_t-\hat{X}(k|k)_{t-1}\right\|}{\left\|\hat{X}(k|k)_{t-1}\right\|} \le \varepsilon$   (25)
        $\hat{X}(k|k) \leftarrow \hat{X}(k|k)_t$
        $\hat{P}(k|k) \leftarrow \hat{P}(k|k)_t$
        break          // Convergence achieved, proceed to Step 7
    else $t \leftarrow t+1$
        continue          // Return to Step 5 for further iterations
7: Iterative filtering process.
    $k \leftarrow k+1$
    Repeat step 2 to step 6 until the filtering is complete.
```

The estimation error covariance $\hat{P}(k|k)$ derived from the MCCEKF reflects the system's estimation accuracy. The optimal waypoints of UAV are achieved by minimizing the trace of this covariance matrix and updating the measurement equations adaptively, thereby enhancing the overall estimation accuracy.

B. Particle Swarm Optimization based Single-Step Path Planning Algorithm

PSO is utilized to optimize the UAV's next waypoints to achieve better estimation accuracy. Each particle in the PSO performs global optimization searches within the solution space to avoid getting trapped in local optima and converge to the optimal value quickly.

Firstly, we initialize a population $N =: (N_1, N_2, \cdots, N_n)$ with n individuals, population dimension $D =: \left[D_\xi, D_\eta\right]^T$, D_ξ and D_η are represented the motion vectors of the UAV along the ξ and η axis respectively. Each particle $\tau(\tau = 1, 2\cdots N)$ in the swarm is characterized by its position and velocity vector. The particle swarm is initialized according to Equations (26) and (27), the position vector $\lambda_{\tau d}(k)$ and velocity vector $\Delta\lambda_{\tau d}(k)$ of the particle at time k are represented as follows:

$$\lambda_{\tau d}(k) = \left[\lambda_{\tau\xi}(k), \lambda_{\tau\eta}(k)\right]^T \tag{26}$$

$$\lambda_{\tau d}(k) = \left[\lambda_{\tau\xi}(k), \lambda_{\tau\eta}(k)\right]^T \tag{27}$$

The magnitude of measurement noise determines the weight allocated to sensor data during the filter's state update when the cost function is defined in the PSO. Proper selection and definition of measurement noise parameters are essential. Specifically, excessive measurement noise may cause the filter to overly prioritize model predictions while disregarding actual measurements, while insufficient noise levels can result in the filter becoming excessively reliant on measurements while neglecting the underlying system model.

The maximum measurement noise is applied to the measurement equation to make the filter more sensitive to measurement data at critical moments by defining a set of $j(j = 1, 2, \cdots 1000)$ measurement noises and maximizing $v_j(k)$, which effectively mitigates large estimation errors in dynamic environments and consequently improves the accuracy of path planning.

The estimated covariance matrix $\hat{P}(k|k)$ represents the tracking accuracy of the maneuvering target, two specific methods are processed to convert the optimization of $\hat{P}(k|k)$ into a scalar value: FIM and Trace. FIM measures the overall uncertainty in high-dimensional states, and a smaller determinant value indicates higher tracking accuracy. The trace serves as a simple scalar measure to quantify the overall level of uncertainty. Trace optimization is typically applied for convex problems, while FIM optimization is applied to non-convex optimization in high dimensions, which lead to local optima. Consequently, we adopt the trace of the covariance matrix as our cost function to characterize the uncertainty in state estimation. The cost function for the next possible waypoint based on current information is minimized to reduce the uncertainty of estimation error.

For ease of understanding, as shown in Table II, the cost function is defined in the PSO algorithm.

TABLE II
THE COST FUNCTION IN PSO

Input: $\hat{X}(k|k-1)$, $\hat{P}(k|k-1)$, $\lambda_{\tau d}(k)$, $\hat{P}(0|0)$

Output: $J(\lambda_{\tau d}(k))$

1: Initialize the particle swarm, the next possible waypoint is represented as:

$$\hat{X}(k|k-1)_{\tau d} = \hat{X}(k|k-1) + \delta_{\tau d}(k) \quad (28)$$

$$\delta_{\tau d}(k) = [\lambda_{\tau\xi}(k), 0, \lambda_{\tau\eta}(k), 0, 0, 0, 0, 0]^T \quad (29)$$

2: Calculate the Jacobian matrix $H(k)_{\tau d}$ according to the current state prediction $\hat{X}(k|k-1)_{\tau d}$ to obtain the following cost function $J(\lambda_{\tau d}(k))$.

$$\begin{aligned} K(k)_{\tau d} &= \hat{P}(k|k-1) H^T(k)_{\tau d} \\ &\left(H(k)\hat{P}(k|k-1)H^T(k)_{\tau d} + R(k)\right)^{-1} \end{aligned} \quad (30)$$

$$\begin{aligned} \hat{P}(k|k)_{\tau d} &= \left(I - K(k)_{\tau d} H(k)_{\tau d}\right)\hat{P}(k|k-1) \\ &\left(I - K(k)_{\tau d} H(k)_{\tau d}\right)^T + K(k)_{\tau d} R(k) K^T(k)_{\tau d} \end{aligned} \quad (31)$$

$$J(\lambda_{\tau d}(k)) = \left\{\max_j \ trace\left\{\hat{P}(k|k)^j_{\tau d}\right\}\right\} \quad (32)$$

The fitness values are evaluated utilizing the cost function formulated in Table II. Through minimization of this cost function, the quality of particle positions is assessed to determine the subsequent optimal waypoints for the UAV. For ease of understanding, Table III delineates the systematic implementation procedure of the UAV path planning algorithm based on PSO. The algorithm encompasses critical PSO components including particle initialization, fitness evaluation, individual and global best position updates, and velocity and position updates. The system progressively converges towards the optimal solution through iterative execution of these algorithmic steps.

TABLE III
ALGORITHM PROCESS OF PSO

Input: $J(\lambda_{\tau d}(k))$, N, D, ϖ, c_1, c_2, $\lambda_{\tau d}(k)$, $\Delta\lambda_{\tau d}(k)$

Output: $\hat{X}'(k)$

1: Initialize parameters. Including inertia weight ϖ, learning factors c_1 and c_2.

2: Prediction. Initialize the position vectors and velocity vectors of each particle randomly. Calculate the fitness value of each particle based on Table II.

3: Update the particle's individual historical optimal position $\lambda_{nd}(k)$, which represents the position $f_{pbest}(k)$ where the particle has found the individual optimal fitness value.

$$\begin{aligned} J(\lambda(k)) &= \min_{\tau}\left\{\max_j \ trace\left\{\hat{P}(k|k)^j_{\tau d}\right\}\right\} \\ &= \min\left\{J(\lambda_{1d}(k)), J(\lambda_{2d}(k)) \cdots, J(\lambda_{ND}(k))\right\} \end{aligned} \quad (33)$$

4: If (34) holds, continue to 5. Otherwise, update the swarm's historical optimal position, which represents the position where the particle has found the swarm's optimal fitness value.

$$J(\lambda(k)) \le J\left(\lambda_{nd}(k)^*\right) \quad (34)$$

$$\lambda_{nd}(k)^* = \lambda(k) \quad (35)$$

5: Update the particle's velocity and position vectors, $k+1 \rightarrow k$ and execute step 3 to perform the next round of optimization.

$$\begin{aligned} \Delta\lambda_{\tau d}(k+1) &= \varpi\Delta\lambda_{\tau d}(k) + c_1\left(\lambda(k) - \lambda_{\tau d}(k)\right) \\ &+ c_2\left(\lambda_{nd}(k)^* - \lambda_{\tau d}(k)\right) \end{aligned} \quad (36)$$

$$\lambda_{\tau d}(k+1) = \lambda_{\tau d}(k) + \Delta\lambda_{\tau d}(k+1) \quad (37)$$

Therefore, the optimal position state $X'(k)$ of the system at step $k+1$ is represented as:

$$X'(k) = \hat{X}(k+1|k) + \left[\lambda_{n\xi}(k)^*, 0, \lambda_{n\eta}(k)^*, 0, 0, 0, 0, 0\right]^T \quad (38)$$

The MCEP algorithm is utilized to improve the tracking accuracy of UAV maneuvering targets. Firstly, MCCEKF is utilized for state and covariance prediction and updates. Secondly, n candidate waypoints are generated utilizing the updated state estimate position as the center point, the trace of the n updated covariance matrix is then computed and serves as the cost function of PSO. The UAV's next optimal position is derived through PSO iteration to correct the system state measurement equation $\hat{Z}'(k)$, this equation is integrated into the MCCEKF to obtain the next optimal state update, thereby significantly enhancing the accuracy of maneuvering target tracking. For ease of understanding, a comprehensive flowchart of the MCEP algorithm is illustrated in Figure 2.

IV. SIMULATION EXPERIMENTS AND ANALYSIS

The simulation examples are provided in order to demonstrate the effectiveness of the proposed algorithms in Section III. The positions of two known static anchor are denoted at $(0,925)m$ and $(200,1050)m$ in a 2D plane $O-\xi\eta$, a moving target with an unknown position departs from $(0,600)m$ with speed $(0.3,0.3)m/s$.

We set sampling time $k=1s$, iteration count $T=600$, particle size $N=70$, particle dimension $D=2$, inertia weight $\varpi=0.5$, learning factors $c_1=2$ and $c_2=2$, $F(k)$ and F_i have been provided in Section II. The process noise covariance $\omega(k) \sim N(0,Q(k))$ and measurement noise $v(k) \sim \beta(k)N(0,0.01)+0.1N(0,0.1)$, $\beta(k)$ follows a Bernoulli distribution with success probability $\varepsilon(k)=0.9$, $\varepsilon(\beta_k=1)=0.9$.

The proposed MCEP algorithm is compared with EKF, MCCEKF, and EKF assisted by the PSO algorithm (abbreviated as EKF-PSO) through simulations. For all algorithms, we set the initial state $\hat{X}(0|0)=[\text{-}1000,10,1200,5,200,0.3,800,0.3]^T$ and the initial covariance $\hat{P}(0|0)=10^3 \times diag\{1,0.01,1,0.01,1,0.01,1,0.01\}$, and the results are presented in Figures 3-7.

A. Comparison of Tracking Trajectory Accuracy among Different Algorithms

Figure 3 illustrates the global trajectory of the system obtained by each algorithm under non-Gaussian noise based on 200 Monte Carlo simulations. This figure depicts the motion trajectories of both the target and the UAV including the actual trajectories and the predicted trajectories.

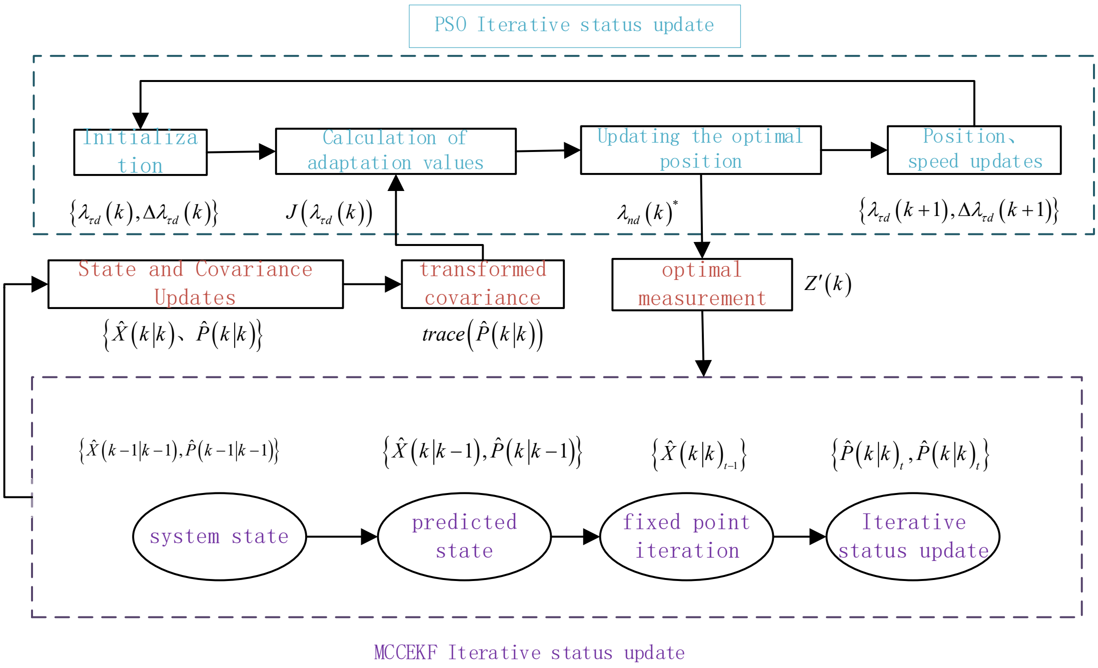
PSO Iterative status update
Initialization
Calculation of adaptation values
Updating the optimal position
Position、speed updates
$\{\lambda_{\tau d}(k),\Delta\lambda_{\tau d}(k)\}$
$J(\lambda_{\tau d}(k))$
$\lambda_{nd}(k)^*$
$\{\lambda_{\tau d}(k+1),\Delta\lambda_{\tau d}(k+1)\}$
State and Covariance Updates
transformed covariance
optimal measurement
$Z'(k)$
$\{\hat{X}(k|k)、\hat{P}(k|k)\}$
$trace(\hat{P}(k|k))$
$\{\hat{X}(k-1|k-1),\hat{P}(k-1|k-1)\}$
$\{\hat{X}(k|k-1),\hat{P}(k|k-1)\}$
$\{\hat{X}(k|k)_{t-1}\}$
$\{\hat{P}(k|k)_t,\hat{P}(k|k)_t\}$
system state
predicted state
fixed point iteration
Iterative status update
MCCEKF Iterative status update

Fig. 2. MCEP algorithm overall flowchart.

As shown in Figure 3, the actual and predicted trajectories of the system exhibit significant differences under varying optimization conditions. In the absence of PSO, the UAV trajectory exhibits substantial oscillations and deviations, particularly pronounced near the terminal point, resulting in notable discrepancies between the predicted trajectories of both the UAV and target. Conversely, the implementation of PSO yields enhanced performance, characterized by a smoother UAV trajectory that demonstrates progressive convergence toward the target path. The high degree of correlation between actual and predicted values for both the UAV and target indicates superior prediction accuracy. This improvement can be attributed to the PSO's ability to effectively mitigate the impact of external environmental perturbations through optimization of the estimated covariance matrix and reduction of noise interference, thereby enhancing both the accuracy of maneuvering target prediction and overall system stability.

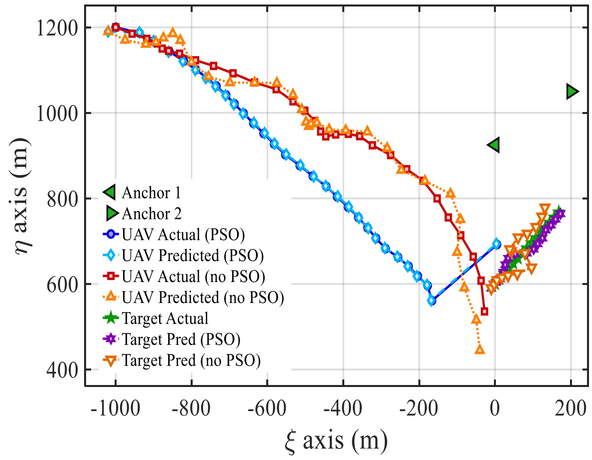

Fig. 3. Global tracking trajectory diagram with and without PSO.

The cost function value which corresponds to the trace of the error covariance matrix, serves as a critical metric for evaluating estimation accuracy. The results demonstrate that a significant reduction in the trace of the error covariance matrix under PSO. By leveraging its global search capability, PSO effectively circumvents local optima, thereby improving parameter adaptability. Furthermore, the smoother and less fluctuating convergence curve of the trace under PSO optimization reflects enhanced filtering stability, attributed to the refined parameter tuning. These findings validate that PSO dynamically adjusts key parameters, achieves an optimal balance between exploration and exploitation, and ultimately enables higher-precision state estimation in complex noise environments and nonlinear systems.

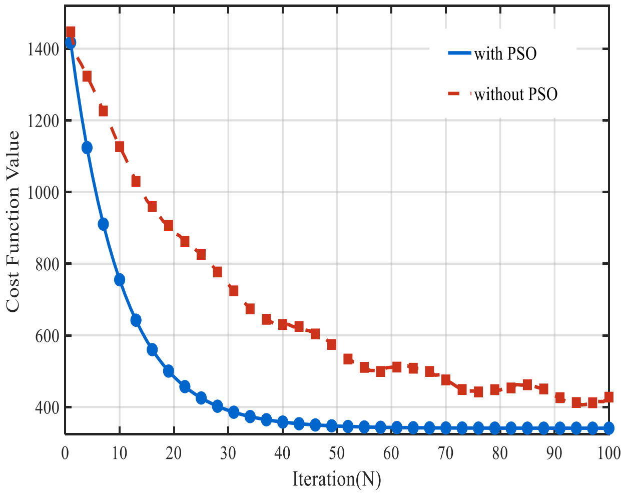

Fig. 4. The cost function value with and without PSO.

Additionally, Figures 5-8 are calculated as the error norms for the position and velocity estimates of the UAV and target, which are defined as the sum of the error components along the ξ and η axis to quantify the deviation between the estimated results and the true values:

$$\|X\|_2=\sqrt{\sum_{i=1}^{n}\left(X_{i\xi}-\hat{X}_{i\xi}\right)^2+\left(X_{i\eta}-\hat{X}_{i\eta}\right)^2} \qquad (39)$$

From Figures 5-8, the proposed MCEP demonstrates consistently superior performance with lower error norms compared to the three benchmark algorithms. Specifically, the target's velocity error norm remains consistently within $0-1.5m/s$, whereas the UAV's velocity error norm ranges from $0-5m/s$ with significant deviations, primarily attributed to abrupt and frequent directional changes in the UAV's velocity vector. Additionally, MCEP effectively addresses both non-Gaussian noise characteristics and system model nonlinearity through simultaneously minimizing the estimation error covariance matrix, which demonstrates that the proposed MCEP achieves higher precision in maneuvering target state estimation.

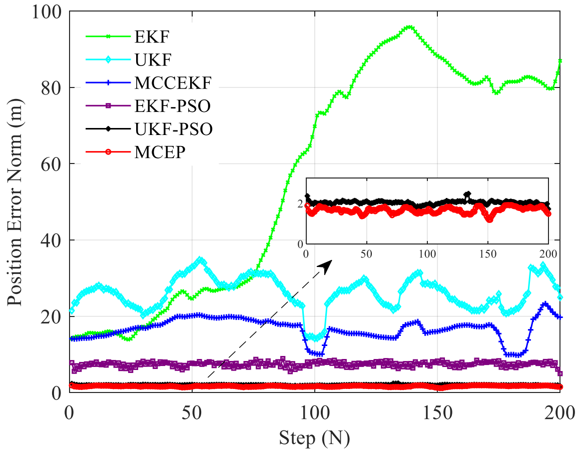

Fig. 5. Position error norm of target.

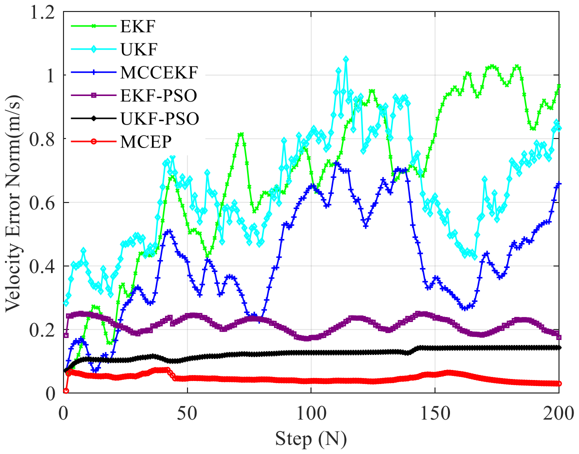

Fig. 6. Velocity error norm of target.

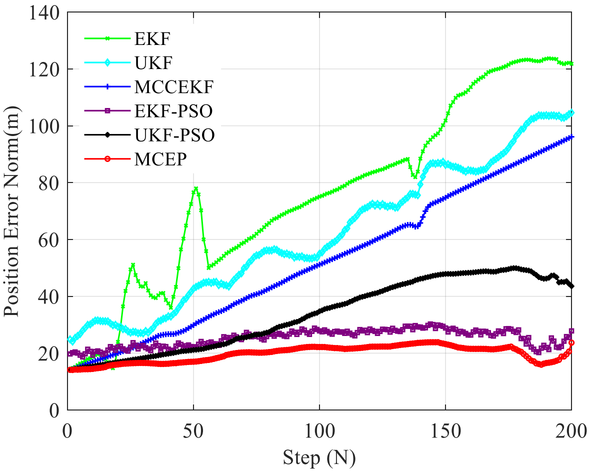

Fig. 7. Position error norm of UAV.

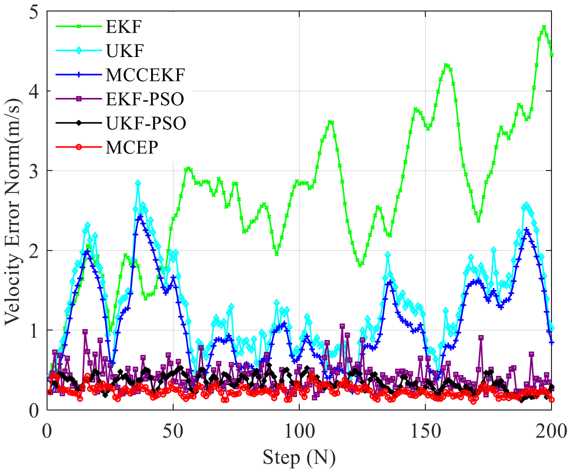

Fig. 8. Velocity error norm of UAV.

A. Comparison of Tracking Accuracy Errors under Different Measurement Noise

Figures 9-16 illustrate the average root mean square error (ARMSEs) curves of four algorithms under varying measurement noise q based on 200 Monte Carlo simulations, which provide a quantitative assessment of the model's prediction accuracy and facilitate performance comparison. The ARMSE is defined as follows:

$$ARMSE=\frac{1}{N}\sum_{i=1}^{N}\sqrt{\frac{1}{n}\sum_{j=1}^{n}\left(X_{ij}-\hat{X}_{ij}\right)^{2}} \tag{40}$$

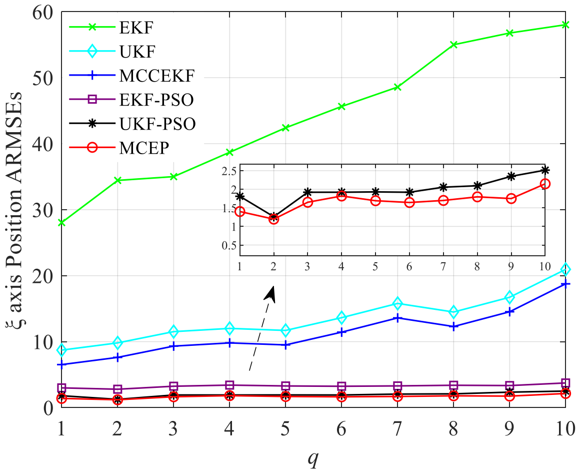

Fig. 9. ARMSEs of target ξ -axis position at different q .

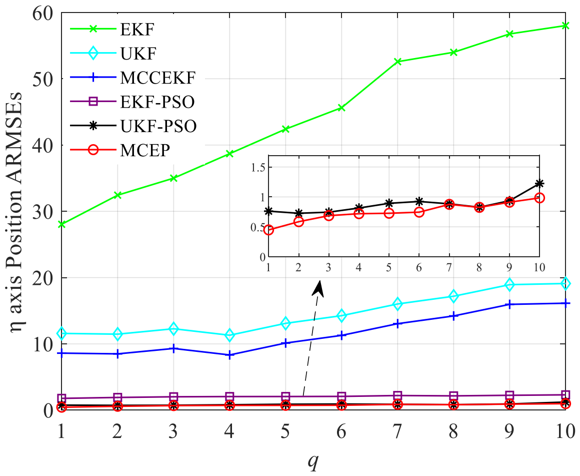

Fig. 10. ARMSEs of target η -axis position at different q .

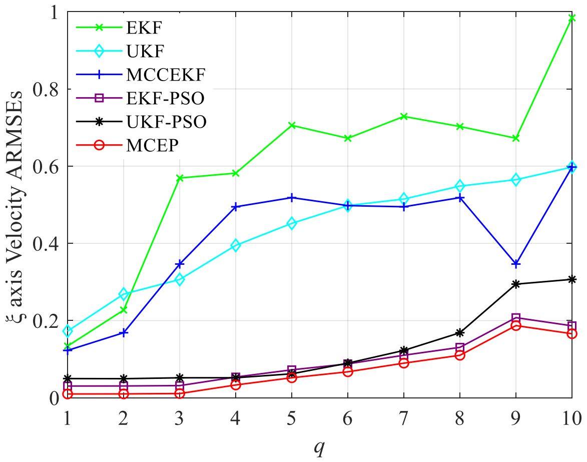

Fig. 11. ARMSEs of target ξ -axis velocity at different q .

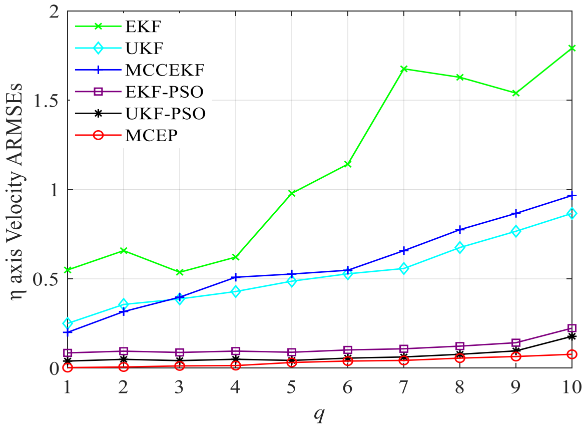

Fig. 12. ARMSEs of target η -axis velocity at different q .

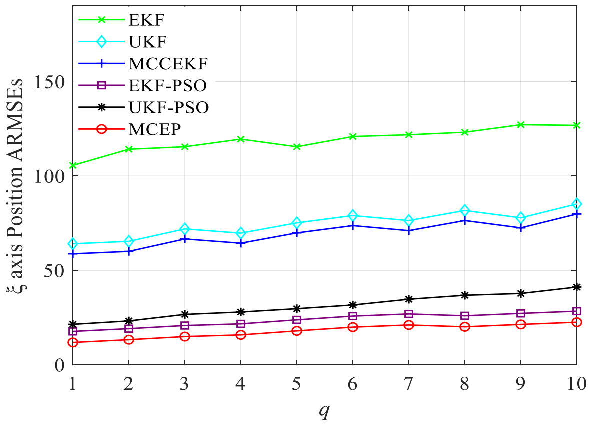

Fig. 13. ARMSEs of UAV ξ -axis position at different q .

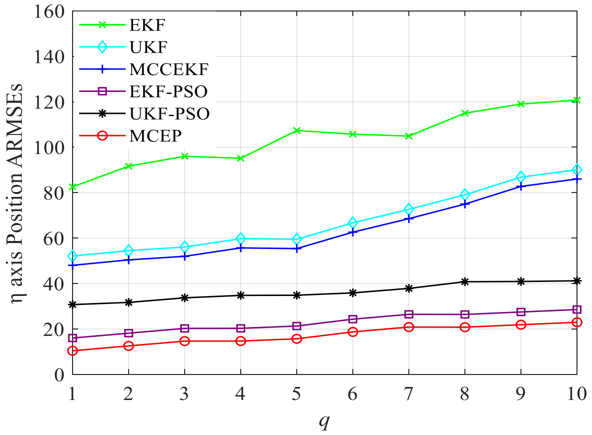

Fig. 14. ARMSEs of UAV η -axis position at different q .

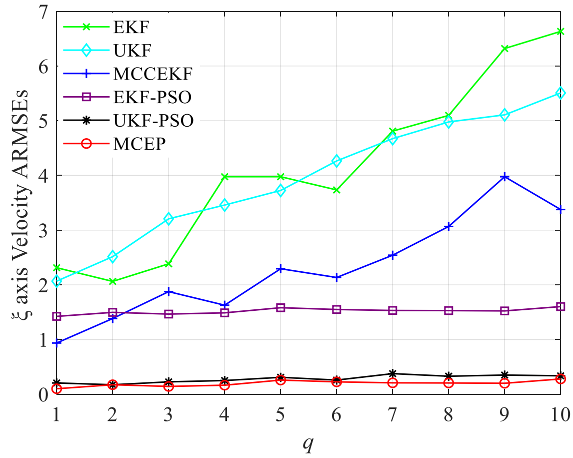

Fig. 15. ARMSEs of UAV ξ -axis velocity at different q .

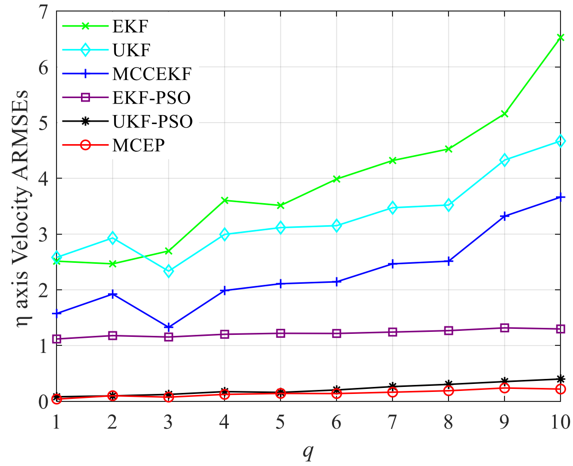

Fig. 16. ARMSEs of UAV η -axis velocity at different q .

Let q increase by 1 each time. As shown in Figures 9-10, a comparative analysis of the ARMSEs for both UAV and target (positions and velocities) along the ξ and η axis is conducted. The ARMSEs for all algorithms gradually increase mildly with elevated noise levels. The proposed MCEP algorithm maintains consistently superior performance with lower error metrics across different noise conditions. MCEP algorithm effectively addresses the challenge of excessive peak tracking errors in maneuvering target scenarios, whereas simultaneously demonstrating enhanced filtering accuracy and robust performance characteristics.

TABLE IV
ARMSEs OF THE COMPARED ALGORITHMS FOR THE TARGET

comparative algorithms	ξ (*m*)	η (*m*)	$\dot{\xi}$ (*m/s*)	$\dot{\eta}$ (*m/s*)
EKF	44.26	44.36	0.59	1.11
UKF	13.34	14.22	0.43	0.53
MCCEKF	11.34	11.55	0.41	0.58
EKF-PSO	3.44	1.83	0.10	0.11
UKF-PSO	1.98	0.87	0.12	0.07
MCEP	1.67	0.75	0.07	0.06

TABLE V
ARMSEs OF THE COMPARED ALGORITHMS FOR THE UAV

comparative algorithms	$\xi\ (m)$	$\eta\ (m)$	$\dot{\xi}\ (m/s)$	$\dot{\eta}\ (m/s)$
EKF	118.99	103.82	4.13	3.93
UKF	74.47	68.43	3.95	3.36
MCCEKF	69.31	63.66	2.32	2.30
EKF-PSO	23.06	23.23	1.53	1.23
UKF-PSO	31.09	36.27	0.28	0.22
MCEP	17.87	17.35	0.20	0.14

Table IV and V compare the ARMSEs of various algorithms for the target and UAV. As shown in Table IV, the MCEP algorithm outperforms all other algorithms in position estimation, achieving the smallest ARMSE. In terms of velocity estimation, MCEP performs slightly better than UKF-PSO, demonstrating its effectiveness. Overall, the proposed algorithm outperforms the individual EKF-PSO and UKF-PSO in both position and velocity estimation, further validating its superior performance. Compared to EKF-PSO and UKF-PSO algorithms, the MCEP algorithm achieves reductions of approximately 55.2% and 34.7% in position and velocity ARMSEs, respectively, further demonstrating its higher tracking accuracy.

As shown in Table V, compared to the target's position and velocity ARMSEs, the UAV's estimation performance in terms of position and velocity is slightly worse, possibly due to the frequent changes in velocity. Compared to EKF-PSO and UKF-PSO algorithms, the MCEP algorithm achieves reductions of approximately 24.3% and 76.9%, 14.6% and 32.4% in position and velocity ARMSEs, respectively, demonstrating higher tracking accuracy.

V. Conclusion

In this paper, we propose MCEP algorithm to solve the problem of nonlinear systems with non-Gaussian noise in GPS-denied environments, aiming to improve the tracking accuracy of UAV. The algorithm leverages the estimated error covariance obtained from MCCEKF as an optimization cost function, while employing Particle Swarm Optimization (PSO) to optimize the UAV's trajectory in the search space for enhanced state estimation accuracy. Through comprehensive simulation studies and comparative analysis against existing algorithms, the effectiveness of the proposed MCEP approach is thoroughly validated. The results demonstrate that by incorporating the MCC criterion for handling non-Gaussian noise and nonlinearity in system models, combined with PSO-based path optimization, the algorithm achieves superior target state estimation in uncertain environments with significantly reduced estimation errors. This enhanced robustness and accuracy makes MCEP particularly suitable for target tracking applications in dynamic systems.

Future research directions will focus on incorporating complex environmental factors in UAV path planning (such as terrain variations and dynamic obstacles) to further optimize the system's adaptability and robustness in practical operational scenarios. We aim to significantly enhance the UAV's path planning capabilities in complex and dynamic environments through these research efforts, thereby providing more reliable solutions for practical applications.

References

[1] Z. Li and H. Wu, "A survey of maneuvering target tracking using Kalman filter," in *Proc. 4th Int. Conf. Mechatronics, Materials, Chemistry and Computer Engineering (ICMMCCE 2015)*, Nanchang, China, 2015, pp. 580-583.

[2] W. Chen, K. Denesh, and E. Janaka, "Hardware implementation and RF high-fidelity modeling of compressive sensing based 2D angle-of-arrival measurement system for 2–18 GHz radar electronic support measures," *Sensors*, vol. 21, no. 20, p. 6823, 2021.

[3] U. Asfia et al., "2D and 3D angles-only target tracking based on maximum correntropy Kalman filters," *Sensors*, vol. 22, no. 15, p. 5625, 2022.

[4] D. Xu et al., "The best-worst method based on interval neutrosophic sets," *IAENG International Journal of Computer Science*, vol. 51, no. 10, pp. 1527-1533, 2024.

[5] G G. Wang, Y. Zhang, and Q. Ai, "Lightweight aerial target detection algorithm with enhanced small target perception," *IAENG International Journal of Computer Science*, vol. 51, no. 12, pp. 2123-2134, 2024.

[6] S. Wang et al., "Optimal geometry and motion coordination for multisensor target tracking with bearings-only measurements," *Sensors*, vol. 23, no. 14, pp. 115-119, 2023.

[7] H. Hu et al., "Robust estimation in continuous–discrete cubature Kalman filters for bearings-only tracking," *Applied Sciences*, vol. 12, no. 16, p. 8167, 2022.

[8] U. Kaba and H. Temeltas, "3D generalized bias compensated pseudolinear Kalman filter for colored noisy bearings-only measurements," *ISA transactions*, vol. 139, pp. 263-271, 2023.

[9] Y. Bai et al., "Research of localization method of coal mine snake detecting robot," *IAENG International Journal of Computer Science*, vol. 51, no. 7, pp. 925-935, 2024.

[10] F. Ni et al., "Cooperative obstacle avoidance planning via A*-BDWA fusion for unmanned aerial vehicles," *IAENG International Journal of Computer Science*, vol. 51, no. 11, pp. 1793-1803, 2024.

[11] X. Feng et al., "Student T-Based maximum correntropy unscented Kalman filter for UAV target tracking," *Unmanned Systems*, vol. 11, no. 4, pp. 115-117, 2023.

[12] U. Asfia and R. Rahul, "Range parameterised maximum correntropy unscented Kalman filter for two dimensional angles-only target tracking problems," *IFAC-PapersOnLine*, vol. 55, no. 22, pp. 218-223, 2022.

[13] S. Li et al., "Minimum error entropy based multiple model estimation for multisensor hybrid uncertain target tracking systems," *Signal Process*, vol.14, no.4, pp.199-213, 2020.

[14] K. Dogancay, "UAV path planning for passive emitter localization," *IEEE Trans. Aerospace and Electronic Systems*, vol.48, no.2, pp.1150-1166, 2012.

[15] K. Dogancay, "3D pseudolinear target motion analysis from angle measurements," *IEEE Trans. Signal Processing*., vol.63, no.6, pp.1570-1580, 2015.

[16] K. Dogancay, "Self-localization from landmark bearings using pseudolinear estimation techniques," *IEEE Trans. Aerospace and Electronic Systems*, vol.50, no.3, pp.2361-2368, 2014.

[17] D. Rachmawati and L. Gustin, "Analysis of Dijkstra's algorithm and A* algorithm in shortest path problem," *Journal of Physics Conference Series*, vol.1566, no.1, p.012061, 2020.

[18] B. Xu, "Precise Path planning and trajectory tracking based on improved A-Star algorithm," *Measurement and Control*, vol.57, no.8, pp.1025-1037, 2024.

[19] B. Li and Y. Wu, "Path planning for UAV ground target tracking via deep reinforcement learning," *IEEE Access*, vol.8, pp.29064-29074, 2020.

[20] A. Sharma et al., "Path planning for multiple targets interception by the swarm of UAVs based on swarm intelligence algorithms: A review," *IETE Technical Review*, vol.39, no.3, pp.675-697, 2022.